Colloids and Surfaces B: Biointerfaces 152 (2017) 152–158

Contents lists available at ScienceDirect

Colloids and Surfaces B: Biointerfaces

journal homepage: www.elsevier.com/locate/colsurfb

Full length article

# Beneficial effect of Cu on Ti-Nb-Ta-Zr sputtered uniform/adhesive gum films accelerating bacterial inactivation under indoor visible light

Akram Alhussein[a,b,*], Sofiane Achache[a,b], Regis Deturche[c], Frederic Sanchette[a,b], Cesar Pulgarin[d], John Kiwi[d], Sami Rtimi[d,**]

[a] ICD-LASMIS, Université de Technologie de Troyes, UMR 6281, CNRS, Antenne de Nogent, Pôle Technologique de Haute-Champagne, 52800 Nogent, France
[b] Nogent International Center for CVD Innovation, LRC CEA-ICD-LASMIS, UTT, Antenne de Nogent, Pôle Technologique de Haute-Champagne, 52800 Nogent, France
[c] ICD-LNIO, Université de Technologie de Troyes, UMR 6281, CNRS, 12 Rue Marie Curie, 10010 Troyes, France
[d] Ecole Polytechnique Fédérale de Lausanne, EPFL-SB-ISIC-GPAO, Station 6, 1015 Lausanne, Switzerland

ARTICLE INFO

*Article history:*
Received 14 November 2016
Received in revised form 10 January 2017
Accepted 12 January 2017
Available online 15 January 2017

*Keywords:*
Titanium based thin films
Copper
Magnetron sputtering
Super-elastic coatings
*E. coli* inactivation
Biointerface
Metallic ions-release

ABSTRACT

This article presents the evidence for the significant effect of copper accelerating the bacterial inactivation on Ti-Nb-Ta-Zr (TNTZ) sputtered films on glass up to a Cu content of 8.3 at.%. These films were deposited by dc magnetron co-sputtering of an alloy target Ti-23Nb-0.7Ta-2Zr (at.%) and a Cu target. The fastest bacterial inactivation of *E. coli* on this later TNTZ-Cu surface proceeded within ~75 min. The films deposited by magnetron sputtering are chemically homogenous. The film roughness evaluated by atomic force spectroscopy (AFM) on the TNTZ-Cu 8.3 at.% Cu sample presented an RMS-value of 20.1 nm being the highest RMS of any Cu-sputtered TNTZ sample. The implication of the RMS value found for this sample leading to the fastest interfacial bacterial inactivation kinetics is also discussed. Values for the Young's modulus and hardness are reported for the TNTZ films in the presence of various Cu-contents. Evaluation of the bacterial inactivation kinetics of *E. coli* under low intensity actinic hospital light and in the dark was carried out. The stable repetitive bacterial inactivation was consistent with the extremely low Cu-ion release from the samples of 0.4 ppb. Evidence is presented by the bacterial inactivation dependence on the applied light intensity for the intervention of Cu as semiconductor CuO during the bacterial inactivation at the TNTZ-Cu interface. The mechanism of CuO-intervention under light is suggested based on the pH/and potential changes registered during bacterial disinfection.



## 1. Introduction

Titanium alloys are widely used in biomedical applications due to their lightness, low Young's modulus (ratio between stress and strain in a material), high strength, excellent biocompatibility and corrosion resistance [1,2]. These properties depend on the alloy chemical composition and stability [3]. β-type titanium alloys present a low Young's modulus due to the low density of the body-centered cubic (bcc) structure. In addition, they are known for their resistance to stress corrosion and to hydrogen embrittlement [4]. Research on the β-type titanium alloys containing non-toxic elements and non-allergic properties has increased rapidly during the past decade. The objective of this research has been to enhance their mechanical properties and super-elastic performance [2–5]. Recently, several quaternary bulk alloys Ti-Nb-Zr-Ta have been developed for use in the biomedical field [6,7]. Among these alloys, the multifunctional Ti-23Nb-0.7Ta-2Zr-1.2O alloy (the composition is in atomic%), called "Gum metal" showed super-elastoplastic behavior at room temperature, high strength and low Young's modulus and was first reported by Saito et al. [8].

Super-elastic thin films can be used for medical applications and/or micro-actuation. For example, the fabrication of stents for neuro-vascular blood vessels and membrane-based micro-pumps employ materials with a high super-elasticity [9].

In the present work, gum metal thin films (GMTF) doped with copper (TNTZ-Cu) were dc magnetron co-sputtered from an alloying target Ti-23Nb-0.7Ta-2Zr (at.%) and a pure Cu target. Previous studies [10–12] show that Cu-ions are responsible for the inacti-

* Corresponding author at: ICD-LASMIS, Université de Technologie de Troyes, UMR 6281, CNRS, Antenne de Nogent, Pôle Technologique de Haute-Champagne, 52800 Nogent, France.
** Corresponding author at: Ecole Polytechnique Fédérale de Lausanne, EPFL-SB-ISIC-GPAO, Station 6, 1015 Lausanne, Switzerland. Tel.: +41 216936150.
*E-mail addresses:* akram.alhussein@utt.fr (A. Alhussein), sami.rtimi@epfl.ch (S. Rtimi).

http://dx.doi.org/10.1016/j.colsurfb.2017.01.020
0927-7765/

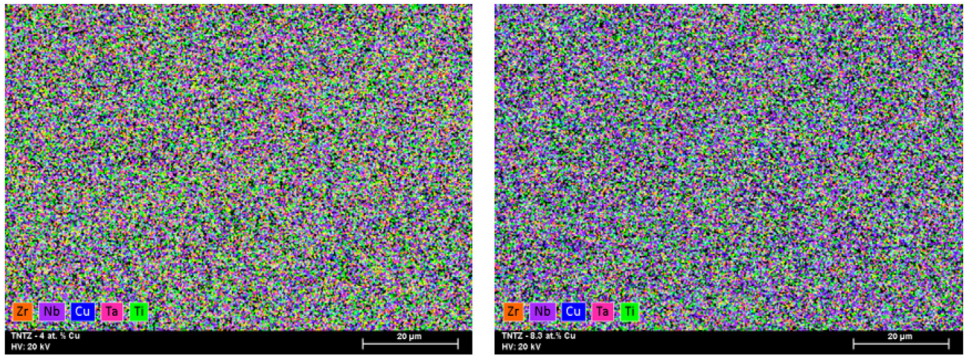


**Fig. 1.** Distribution of the Ti, Nb, Zr, Ta and Cu in films: a) TNTZ-$(Cu)_4$ and b) TNTZ-$(Cu)_8$.

**Table 1**
Chemical composition of TNTZ-$(Cu)_x$ thin films (at.%).

| Sample | TNTZ target | | Ti | Nb | Ta | Zr | Cu |
|---|---|---|---|---|---|---|---|
| | Current (A) | Power (W) | | | | | |
| TNTZ | 0.96 | 228 | 81.1 | 17.4 | 0.6 | 0.9 | 0 |
| TNTZ-$(Cu)_4$ | 1.71 | 441 | 77.2 | 16.8 | 0.9 | 1.1 | 4.0 |
| TNTZ-$(Cu)_7$ | 1.46 | 376 | 74.6 | 16.4 | 0.9 | 1.1 | 7.0 |
| TNTZ-$(Cu)_8$ | 1.20 | 309 | 73.5 | 16.2 | 1.0 | 1.0 | 8.3 |
| TNTZ-$(Cu)_{12}$ | 0.96 | 247 | 69.0 | 16.1 | 1.2 | 0.9 | 12.8 |
| TNTZ-$(Cu)_{18}$ | 0.71 | 171 | 62.5 | 16.1 | 1.8 | 1.0 | 18.6 |

vation of bacteria (e.g.; *E. coli*). Many copper-based coatings e.g.; $TiO_2$-Cu and Cu, Ti, Nb and their oxides were developed and investigated for their antibacterial properties. Achache et al. [13,14] have recently reported the mechanical properties of super-elastic Ti-based gum metal thin films showing increased bacterial inactivation properties and biocompatibility [15,16].

The present study focuses on the effect of copper content on the structure, morphology and mechanical properties of these as-deposited films. Composition, structure, morphology, hardness and Young's modulus are reported. The bactericidal activity of the sputtered films is evaluated for different samples in the dark and under light irradiation. The interfacial interaction, potential and pH on the sputtered films are reported within the disinfection time for these innovative TNZT-Cu coatings.

## 2. Experimental details

### 2.1. Deposition of TNZT-(Cu) films: procedures

Gum metal thin films (GMTF) were deposited on glass and silicon substrates at room temperature by dc magnetron sputtering from two targets: Ti-23Nb-0.7Ta-2Zr (at.%) and pure Cu. Supplementary material 1 shows two similar magnetrons joined to rectangular targets 200 × 100 × 6 mm in size. The chamber was evacuated down to a pressure of $4 \times 10^{-4}$ Pa. The target to sample distance was kept constant at 8 cm. After initial optimization, sputtering was carried out for 2 h leading to films with thickness in the range 1–2 μm. The sample holder rotation speed was set at 12 rpm. The working pressure was kept at 0.85 Pa using constant argon flow rate of 80 sccm. The substrates' bias voltage was −150 V (RF power supply, 40 W, frequency 13.56 MHz). The TNTZ-Cu thin films were deposited applying a constant discharge current of 0.04 A (522 V, 21 W) to the Cu target. The TNTZ target current was varied between 0.71 A and 1.71 A as shown in Table 1.

### 2.2. Physico-chemical characterization of the sample surface properties by EDX, SEM, AFM, XRD and nanoindentation

The chemical composition and distribution of the Ti, Nb, Zr, Ta and Cu in the GMTF were obtained by Energy Dispersive X-ray Spectroscopy (EDX). The TNZT-Cu cross-section images were obtained by scanning electron microscope (SEM) in a Hitachi SU8030 electron microscope. The chemical composition was quantified by Quantax Esprit software. For each sample, the measurement was carried out on multiple zones of the sample showing significant homogeneity. The elements spectra were acquired from SEM images applying a high accelerating voltage of 20 KV and a pressure vacuum of $10^{-4}$ Pa considering: 60 kcps count mode, 40 KeV acquisition range and 2 kcps initial counting rate. The surface topography and RMS roughness of the thin films were obtained by atomic force microscopy (Agilent Technologies 5100 AFM). The AFM 3D-images were acquired in non-contact mode at the resonance frequency of the silicon tip and with set point fixed at 10% of the maximum amplitude. We used an ultra-sharp silicon tip with a shape factor adapted to the morphology of the sample. Images of 256 × 256 pixels were indexed with a scanning speed of 0.4 s/line (acquisition of 256 points/line).

The crystallographic structure of the samples was investigated by X-ray diffraction (XRD) by means of a Bruker D8 Advance instrument (CuKα radiation line). Young's modulus and hardness were obtained by means of a Nano Indenter XP, MTS Systems Corporation with continuous stiffness measurement (CSM) provided for with a three-sided pyramidal diamond tip (Berkovitch). The average of ten indents was taken to determine the values of hardness and Young's modulus. The penetration depth was kept <10% of the film thickness, to minimize the effect of the substrate stiffness.

### 2.3. Bacterial inactivation, irradiation procedures, interfacial surface potential/pH and ion-release evaluated by inductively coupled plasma mass-spectrometry (ICPMS–MS)

*Escherichia coli* (*E. coli* K12) was obtained from the Deutsche Sammlung von Mikroorganismen und Zellkulturen GmbH (DSMZ), Braunschweig (Germany). Coatings' surfaces were sterilized by keeping them in an oven at 80 °C overnight. 100 μL culture aliquots with an initial concentration of $3 \times 10^6$ CFU $mL^{-1}$ in NaCl/KCl (8/0.8 g/$L^{-1}$, pH 7.2) were placed on the coated and uncoated (control) samples. Experiments were run at room temperature and the samples were placed on glass Petri dishes provided with a lid to prevent evaporation during illumination. Then, the samples were transferred into a sterile tube containing NaCl/KCl saline solution and subsequently mixed thoroughly using a Vortex for 2 min. Serial dilutions were made in NaCl/KCl solution. A 100 μL sample of each dilution was pipetted onto a nutrient agar plate and spread over the

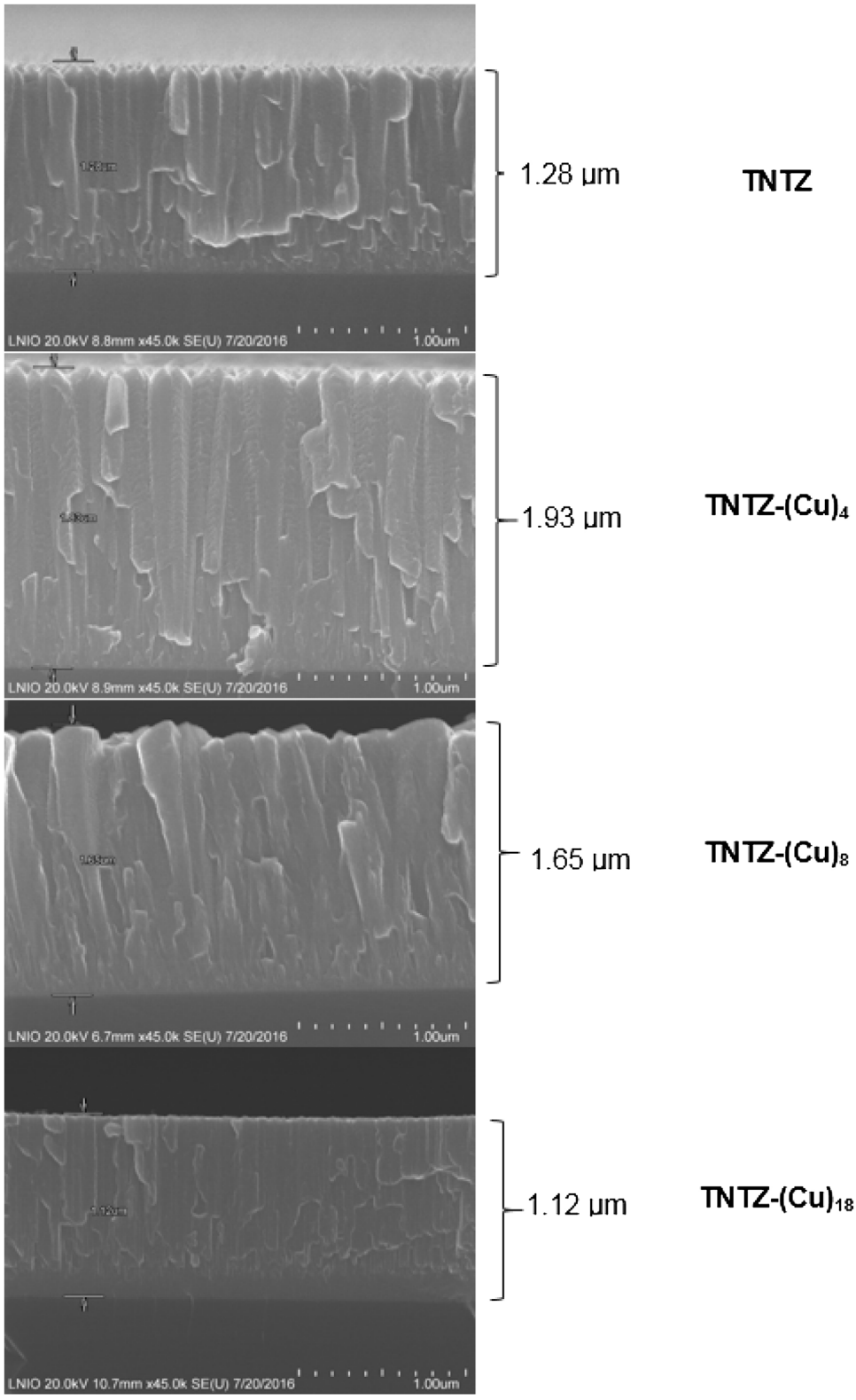


**Fig. 2.** Cross-section SEM images of TNTZ-films with different Cu at.%.

surface of the plate using the standard plate method. Agar plates were incubated lid down, at 37 °C for 24 h before the CFU counting. Three independent assays were done for each sample. The statistical analysis of the results was performed for the CFU values calculating the standard deviation (n = 5%). The average values were compared by one-way analysis of variance with the values of statistical significance. Irradiation of the samples was carried out in a cavity provided with tubular actinic Osram Lumilux 18W/827 emitting in the range 360–700 nm with an integral output of 5 mW/cm$^2$ as measured by Global and UV radiometer Kipp & Zonen Mod. CM3 and CUV3.

The interfacial potential and pH were followed on a Jenco 6230N micro-electrode, San Diego, USA (provided for with a microprocessor and a RS-232-C IBM interface). The redox potential and pH were measured using the nano-volt/micro-Ohm meter with platinum electrodes and the pH of the sputtered surface. The pH meter was able to record the pH-changes in the seconds scale with a high degree of pH sensitivity of 0.01 pH units. The electrode was immersed in the bacterial suspension on the sample and the measurements were taken after a suitable delay required for the measurement stabilization.

A Finnigan™ Inductive coupled plasma mass spectrometer (ICP-MS) was used to detect the Ti, Nb, Ta, Zr and Cu released during the bacterial loss of viability runs. This instrument was equipped with a double focusing reverse geometry mass spectrometer having an extremely low background signal and high ion-transmission coefficient. The spectral signal resolution was $1.2 \times 10^5$ cps/ppb and the detection limit of 0.2 ppb.

## 3. Results and discussions

### 3.1. EDX determination of the film composition and surface distribution

Table 1 shows the chemical compositions of the TNTZ-$(Cu)_x$ films as determined by EDX. The chemical homogeneity of the films is shown in Fig. 1. The copper content is controlled via the discharge current applied to the TNTZ target. The Cu target current was kept constant at 0.04 A during all the deposition processes of TNTZ-(Cu) films. This method was used because of the high sputter yield of copper compared to that of other elements.

From Table 1, it can be seen that chemical composition in the TNTZ-$(Cu)_x$ films are not similar to those in the Ti-23Nb-0.7Ta-2Zr (at.%) target. Increasing the current applied to the TNTZ target leads to rise the Ti content in the film. The Cu content in the film is balanced with that of the Ti. The low Nb and Zr contents in the films (respectively ~16 at.% and 1 at.%) compared to that of the target (respectively ~23 at.% and 2 at.%) could be due to the re-sputtering of these elements by the argon ions when the bias was kept at a high level (−150 V) while the Cu-content increased up to 18.6 at.% and the Ti-content decreased from 81.1 at.% to 62.5 at.%.

Fig. 1 represents the distribution of the elements in films TNTZ-$(Cu)_4$ and TNTZ-$(Cu)_8$ with the values shown in Table 1. The Ti, Nb, Ta, Zr and Cu identified with different colors in Fig. 1 are seen to be homogeneously distributed in both cases on the film surface as expected for coatings deposited by a standard magnetron sputtering method.

### 3.2. Morphology and surface topography of films observed by SEM and AFM

Fig. 2 shows fractured cross-sectional SEM images of 4 sputtered TNTZ-(Cu) samples with different amounts of Cu. The films present a columnar morphology due to the high deposition pressure (0.85 Pa) leading to a loss of adatoms energy and surface mobility as a consequence of the collision with argon-ions in the plasma (see Experimental details).

Fig. 3 shows the topography of the samples using atomic force microscopy (AFM). The 3D surface mappings of the TNTZ-(Cu) films are presented. The roughness (RMS) and the roughness average values of the six different TNTZ-$(Cu)_x$ samples are presented in Supplementary material 2. The RMS values quantified the vertical deviations of a real surface from its ideal form and provide a measure of the surface roughness (see Fig. 3). The TNTZ-$(Cu)_8$ sample presenting an RMS roughness of 20.1 nm leads to the fastest bacterial inactivation (see Section 3.4). The topographic AFM *contour* in this case was made up by deep and wide valleys to accommodate the *E. coli* bacteria compared to the TNTZ samples with an RMS roughness value of only 7.38 nm. This RMS value indicates that the AFM contour was made up of close peaks at relatively small distances to each other. The implications for the bacterial inactivation kinetics will be addressed in detail when discussing the bacterial interaction with the TNTZ-$(Cu)_x$ surfaces in Section 3.5. The sample roughness will be shown to play an important role in determining the time of *E. coli* inactivation and is a measure on how the TNTZ-$(Cu)_x$ samples interacts with its environment.

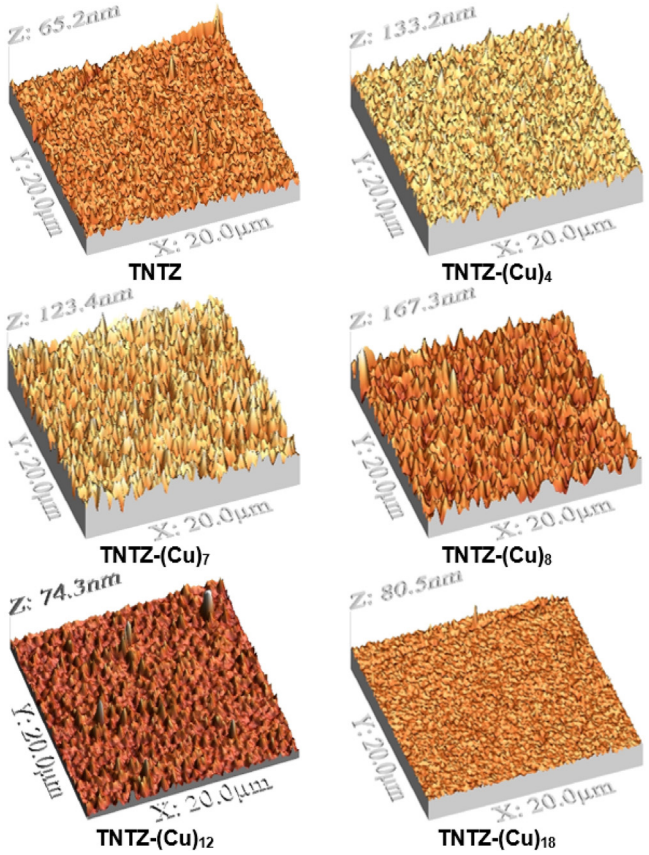


**Fig. 3.** Atomic fore microscopy (AFM) in 3 dimensions of TNTZ and TNTZ-$(Cu)_x$ films.

**Table 2**
Mechanical properties of TNTZ-$(Cu)_x$ thin films.

| Sample | E (GPa) | SD (E) | Hardness (Gpa) | SD (H) |
|---|---|---|---|---|
| TNTZ | 96.7 | 10 | 4.59 | 0.96 |
| TNTZ-$(Cu)_4$ | 94.3 | 18.2 | 4.35 | 1.47 |
| TNTZ-$(Cu)_7$ | 76.6 | 24.1 | 2.98 | 1.37 |
| TNTZ-$(Cu)_8$ | 91.0 | 21.6 | 4.58 | 1.94 |
| TNTZ-$(Cu)_{12}$ | 100.4 | 22.8 | 6.17 | 2.11 |
| TNTZ-$(Cu)_{18}$ | 104.2 | 1.7 | 6.37 | 0.19 |

### 3.3. Microstructure, Young's modulus and hardness

Fig. 4a clearly shows that the films are single phased with the β-Ti BCC structure. The broadening of the (110) peak suggests a decrease of the mean grains size when the copper content increases. This broadening of the TNTZ-$(Cu)_x$ peaks becomes more significant for samples with a Cu content of 12.8 at.% or higher leading to samples presenting a quasi-amorphous structure.

The mechanical properties obtained from nano-indentation measurements of TNTZ and TNTZ-$(Cu)_x$ films are shown in Table 2. Fig. 4b represents the variation of TNTZ-$(Cu)_x$ films properties in

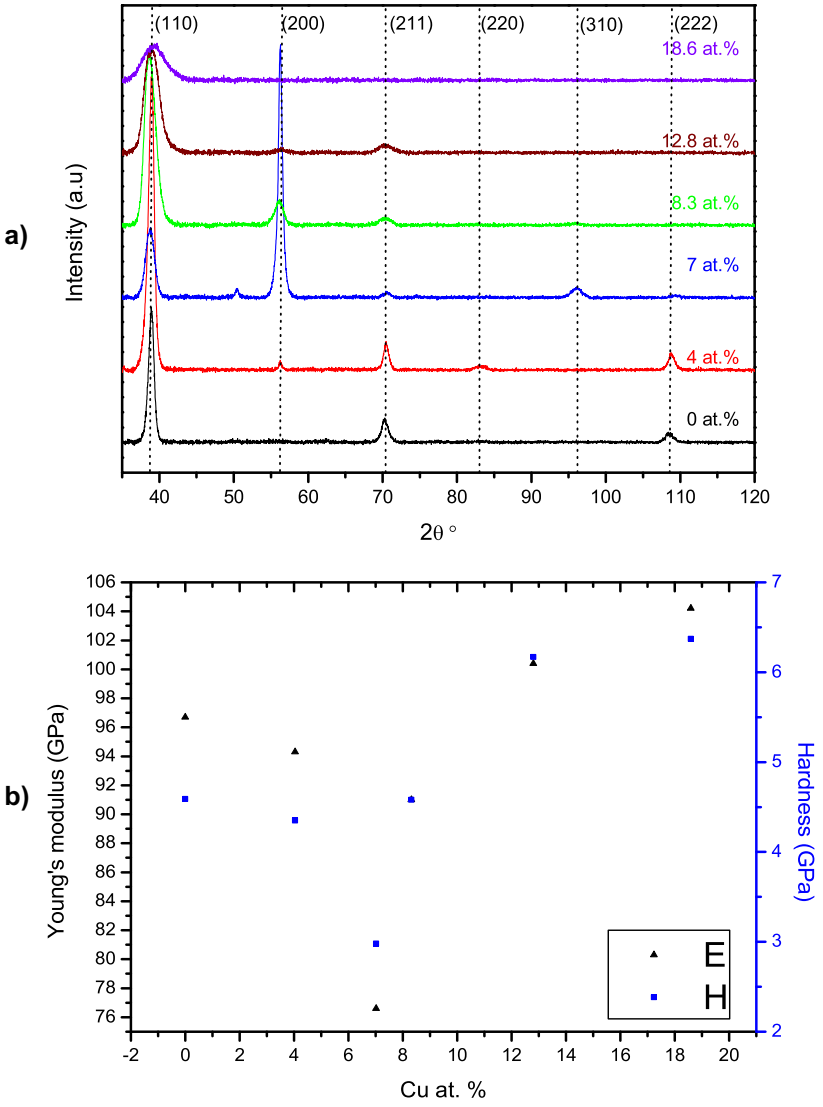


**Fig. 4.** a) X-ray diffraction (XRD) spectrograms of TNTZ-$(Cu)_x$ of samples presenting various copper contents. b) Young's modulus and hardness of TNTZ-$(Cu)_x$ films presenting copper contents as noted in the x-axis.

terms of Young's modulus (E) and hardness (H) as a function of the copper content. E and H vary respectively in the range 77–104 GPa and 3–6.4 GPa by increasing Cu content up to 18.6 at.%. E and H decrease up to a copper content of ~7%, and increase above. Increasing Young's modulus and hardness of TNTZ thin film, containing more than 7 at.% of copper may be assigned to the formation of an amorphous phase. It is readily seen from Table 2 and Fig. 4a and b that the TNTZ-$(Cu)_{18}$ quasi-amorphous has the highest E and H values.

### 3.4. Bacterial inactivation and ions release as detected by ICP–MS

Fig. 5a shows the antibacterial activity of TNTZ and TNTZ-$(Cu)_x$ samples. Cu added to the TNTZ-microstructure as shown in Fig. 5a led to an acceleration of the bacterial inactivation kinetics. Fig. 5a, trace 1) induced the fastest bacterial degradation kinetics. TNTZ-$(Cu)_8$ with an 8.3 at% Cu-content contains the highest amount of Cu-sites in exposed positions interacting with bacteria. Fig. 5a, traces 3) and 4) with a higher Cu content of 12.8 at.% and 18.6 at.% respectively compared to the TNTZ-$(Cu)_8$ sample led to a slower degradation kinetics. The slower degradation kinetics could be rationalized by the following observations: **a**) that the Cu-concentration would be lower at surface level decreasing the number of catalytic sites interacting with bacteria, **b**) the higher doping of Cu% changes the microstructure of the film hindering the diffusion of charges leading to bacterial inactivation. On thicker coatings, the surface Cu-ions would decrease due to the inward back diffusion towards the substrate. These Cu-ions play a major role in the electrostatic interaction of the TNTZ-$(Cu)_x$ with bacteria, **c**) the TNTZ-$(Cu)_8$ presents an RMS roughness of 20.8 nm, this is the largest RMNS value of all the NTNZT-films. A higher RMS means that this surface is made up by higher density peaks leading to accommodate/interact with *E. coli* compared to the rest of the TNTZ-films (see Supplementary material 2) and **d**) the XRD-spectrograms in Fig. 4a show that a Cu presence >8.3% led to a lost in sample crystallinity which plays an important role in the microstructure of the samples leading to bacterial inactivation. Fig. 5a, traces 2) and 5) shows those samples with a Cu content below 4 at.% induce a slower bacterial inactivation of *E. coli* possibly due to the lower Cu-content present in these samples compared to the TNTZ-$(Cu)_8$ sample. The TNTZ sample in Fig. 5a, trace 6) shows almost no bacterial inactivation under light as it was the case for the TNTZ-$(Cu)_8$ sample in the dark. Generally, the interactions between coating and bacteria have been shown to depend on the contact surface size,

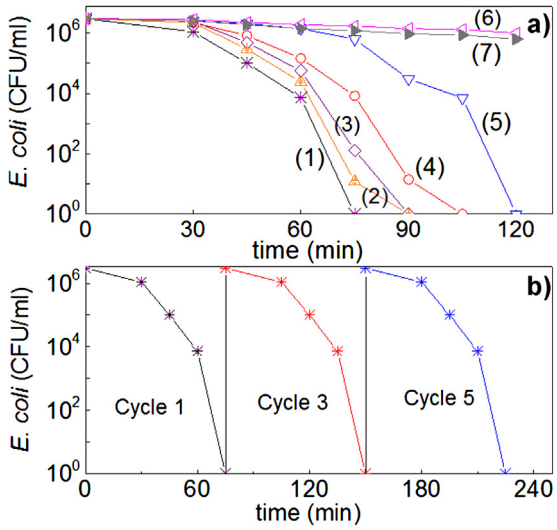


**Fig. 5.** a *E. coli* inactivation on TNTZ-$(Cu)_x$ under actinic Osram Lumilux 18/827 light (5 mW/cm$^2$): 1) TNTZ-$(Cu)_8$ Cu 8.32%, 2) TNTZ-$(Cu)_7$ Cu 7.02%, 3) TNTZ-$(Cu)_{12}$ Cu 12.80%, 4) TNTZ-$(Cu)_{18}$ Cu 18.59%, 5) TNTZ-$(Cu)_4$ Cu 4.04%, 6) TNTZ, Cu zero% and 7) TNTZ-$(Cu)_8$ Cu 8.32% in the dark. Error bars: standard deviation (n = 5%). b *E. coli* inactivation on TNTZ-$(Cu)_8$ up to 5 cycles under similar experimental conditions as used in Fig. 5a. Error bars: standard deviation (n = 5%).

redox potentials and hydrophilic-hydrophobic properties [10,11]. In this study we have shown that the RMS roughness (Fig. 3/discussion) and the crystallization degree of TNTZ-(Cu) obtained by XRD (Fig. 4a/discussion) play an important role controlling the activity of the TNTZ-$(Cu)_x$ surface leading to bacterial inactivation [15].

Fig. 5b shows the recycling up to the 5th cycle of the TNTZ-$(Cu)_8$ leading to bacterial inactivation presenting a stable repetitive kinetics. By Inductive coupled plasma mass-spectrometry (ICP–MS) it is shown that a sample TNTZ-$(Cu)_8$ after the 5th cycle releases only 0.4 ppb (see Supplementary material 3). This amount is far below the cytotoxic level causing damage to mammalian cell as reported recently [16,17]. The Cu-release in the ppb-range allows for a stable performance of this photocatalyst during repetitive bacterial inactivation. Moreover, the interaction between the Cu-ions and the bacteria seems to proceed through an oligodynamic effect. The oligodynamic effect consists of bactericide effect induced by an extremely low concentration of metal/metal-ion [18,19].

The formation of $TiO_2$ and concomitantly $ZrO_2$, $Nb_2O_5$ and $Ta_2O_5$ on the glass with TNTZ-$(Cu)_8$ is due to two different effects: a) the partial oxidation of Ti in the sputtering chamber in the presence of an oxygen source. The residual $H_2O$ vapor in a sputtering chamber at the pressure of $P_{residual} = 4 \times 10^{-4}$ Pa (as noted in the experimental part Section 2.1) is the source of the $O_2$. This pressure allows for the presence of $\sim 10^{15}$ molecules/cm$^2$ of $H_2O$. This is equivalent to a monolayer of water sufficient to generate the $O_2$ to oxidize the Ti-sputtered thin film to $TiO_2$ and b) the films also oxidize after the sputtering is over when exposed to air. In addition, autoclaving at 121 °C during the sterilization process prior to the use of the coating leads to surface oxidation.

In the presence of Ti, Nb, Zr and Cu-oxides, the bacterial inactivation on the TNTZ-$(Cu)_8$ photocatalyst showed an increase with the applied light intensity (see Supplementary material 4). This lends further support for the TNTZ-$(Cu)_8$ composite behaving as a semiconductor. The photo-induced generation of charges increases with a higher light intensity. Cu added to TNZT drastically accelerates the bacterial inactivation as shown in Fig. 5a, trace (1) compared to the data shown in Fig. 5a, trace (6) for TNZT without any Cu-doping. A simplified mechanism on TNTZ-$(Cu)_x$ leading to bacterial inactivation, can be suggested considering CuO as a semiconductor and not based on the Cu content in the TNTZ-$(Cu)_x$ in Table 1. An increase in the Cu-percentage in TNTZ-$(Cu)_x$ did not lead to an acceleration of the bacterial inactivation kinetics as shown in Fig. 5a. If this would be the case, the amount of Cu-charged species (ions) in eq.(1) would increase with a bigger Cu amount. This was not observed.

Visible light photons reaching the TNTZ-CuOx lead to the reaction (1) being CuO a p-type semiconductor with a band-gap of 1.7 eV (cb −0.3 eV and bg 1.4 eV SCE) [20]:

$$CuO + light < 660\,nm \rightarrow CuOe^{-}cb + CuOh^{+}vb \quad (1)$$

A simplified mechanism can be suggested for the generation of highly oxidative intermediates following Eq. (1). In Eq. (1), e-cb refers to conduction band electron and h + vb refers to valence band hole in CuO. The photo-induced CuOe-cb electron reacts with $O_2$ leading to $O_2^-$ as noted in Eq. (2) or reduce $Cu^{2+}$ in the CuO lattice to $Cu^+$ Eq. (3) [21–23]:

$$CuO(e^{-}{}_{cb}) + O_2 \rightarrow CuO + O^{-}{}_2 \quad (2)$$

$$CuO(e^{-}cb) \rightarrow (Cu^{+}O)^{-} \quad (3)$$

Additional $O_2^-$ radicals may also be generated as noted in Eq. (4) [24]:

$$CuO(Cu^{+}) + O_2 \rightarrow CuO(Cu^{2+}) + O^{-}{}_2 \quad (4)$$

The $O^-{}_2$ in Eq. (4) leads to the $HO_2^{\bullet}$ radicals shown in Eq. (5):

$$H^{+} + O_2^{-} \Leftrightarrow HO_2^{\bullet}(partialO^{-}{}_2) pK_a = 4.8 \quad (5)$$

The Cu-leaching during bacterial inactivation was negligible as reported previously by ICP-MS (Supplementary material 3). This suggest that Eq. (3) is much faster compared to the CuO dissolution noted in reaction (6):

$$CuO(Cu^{+}) \rightarrow CuO_{vacancy} + Cu^{+} \quad (6)$$

The mechanism in Eqs. ((1)–(6)) suggests the generation of oxidative radicals by oxidized TNTZ under band-gaps irradiation. We tried to identify the reactive species responsible for the bacterial oxidation on the TNTZ-Cu surface. The results were unclear since the used scavengers may interact differently with the present species on the surface. For example, EDTA has repeatedly been used as hole-scavenger in the case of $TiO_2$ photocatalysis. But it may not play the same role in the case of copper oxide when scavenging the $CuOh^{+}vb$ in reaction (1) [21,22]. Therefore, we cannot identify unambiguously the electronic hole ($h^+$) in reaction (1). Semiconductor sputtered surfaces activity leading to bacterial inactivation under light and in the dark has been recently reported by studies addressing $TiO_2$ and CuO [23–25] and by $ZrO_2$ and $Ta_2O_5$ mediated bacterial inactivation [26].

### 3.5. Surface potential and pH in situ determination during bacterial disinfection

Fig. 6a shows that during the period of bacterial inactivation under actinic light irradiation the pH of 6.85 decreases to 6.41 within 20 min. This is due to the production of long-lived carboxylic acids intermediates during bacterial oxidation on TNTZ-$(Cu)_{8\%}$. The short chain carboxylic acids (branched or not) generated during the bacterial inactivation presented a $pK_a \sim 3$. Subsequently, the pH increases to 6.81 when the carboxylic acids decompose generating $CO_2$. The change in pH was close to a five-fold increase in the concentrations of $H^+$ as shown in the right hand y-axis in Fig. 6a. But after 20 min, the pH increases again up to a pH ~6.81 when the carboxylic acids are being mineralized to $CO_2$. This is the final step in the mineralization of organic compounds by the way of the photo-Kolbe reaction [27,28]. In the dark, the pH values during the bacterial inactivation on TNTZ-$(Cu)_{8\%}$ did not significantly vary and

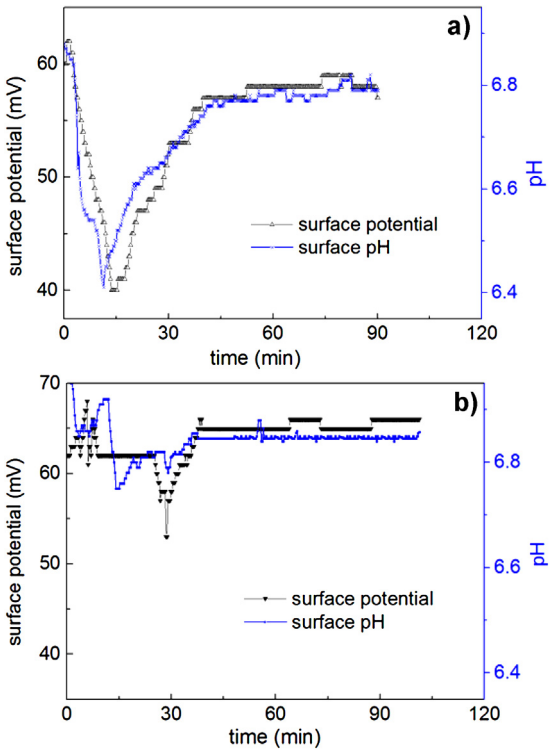


**Fig. 6.** Surface potential and pH during *E. coli* inactivation on TNTZ-$(Cu)_8$ under: a) light (5 mW/cm$^2$) and b) in the dark.

decreased from 6.92 to 6.79 as shown in Fig. 6b due to the slow bactericidal activity in the dark. This was shown by the reduction of the CFU/ml reported in Fig. 5a.

The interfacial potential of the TNTZ-$(Cu)_{8\%}$ sputtered film decreases during bacterial oxidation as shown in Fig. 6a. This leads to the increase of permeability of the outer cell-wall allowing the leak of $K^+$, $Cl^-$, and $Na^+$. The increase in cell wall permeability precludes a normal exchange of vital ions in and out of the cytoplasm. The interfacial potential changes under light were more significant compared to the changes in the dark, which were seen to be small.

## 4. Conclusions

Super-elastic titanium based thin films TNTZ-(Cu) were deposited by DC magnetron sputtering (DCMS). These films contained amounts of copper varying from 4 to 18.6 at.%. The formation of Ti,Nb, Zr and Ta-oxides was explained based on the experimental conditions used in the sputtering chamber. The variation of copper percentage from 4 to 18.6 at.% influences the Young's modulus and hardness of the TNTZ-$(Cu)_x$ gum metal films. It seems that formation of an amorphous phase leads to increasing mechanical properties. The columnar morphology of TNTZ-$(Cu)_8$ obtained by SEM in the sputtered films was due to the high deposition pressure in the magnetron chamber. TNTZ-films with a copper content of 8.3 at.% showed the fastest bactericidal activity under low intensity actinic/indoor light. The bacterial fast inactivation kinetics found by the TNTZ-$(Cu)_8$ was correlated to the at.% Cu, the RMS and the Cu-crystal lattice detected by XRD making this material. The mechanism of bacterial inactivation seems to involve an oligodynamic effect due to the small amount of ions released during disinfection detected by ICP-MS. The antibacterial performance of these films suggests a potential application in hospitals, health care facilities, implants, schools and public places.

## Acknowledgements

We thank EPFL and Swiss National Science Foundation (FNS) project (200021-143283/1) for financial support.

## Appendix A. Supplementary data

Supplementary data associated with this article can be found, in the online version, at http://dx.doi.org/10.1016/j.colsurfb.2017.01.020.

## References

[1] H.Y. Kim, T. Sasaki, K. Okutsu, J.I. Kim, T. Inamura, H. Hosoda, S. Miyazaki, Acta Mater. 54 (2006) 423–433.
[2] M. Tane, S. Akita, T. Nakano, K. Hagihara, Y. Umakoshi, M. Niinomi, H. Nakajima, Acta Mater. 56 (2008) 2856–2863.
[3] Q.M. Hu, S.J. Li, Y.L. Hao, R. Yang, B. Johansson, L. Vitos, Appl. Phys. Lett. 93 (2008) 121902.
[4] S.J. Li, T.C. Cui, Y.L. Hao, R. Yang, Acta Biomater. 4 (2008) 305–317.
[5] S.K. Sikka, Y.K. Vohra, R. Chidambaram, Prog. Mater. Sci. 27 (1982) 245–310.
[6] M. Niinomi, Biomaterials 24 (2003) 2673–2683.
[7] P. Laheurte, F. Prima, A. Eberhardt, T. Gloriant, M. Wary, E. Patoor, J. Mech. Behav. Biomed. Mater. 3 (2010) 565–573.
[8] T. Saito, T. Furuta, J.H. Hwang, S. Kuramoto, K. Nishino, N. Suzuki, Science 300 (2003) 464.
[9] K. Otsuka, X. Ren, Intermetallics 7 (1999) 511.
[10] S. Rtimi, S. Giannakis, R. Sanjines, C. Pulgarin, M. Bensimon, J. Kiwi, Appl. Catal. B: Environ. (2016) 277–285.
[11] V. Stranak, H. Wulff, H. Rebl, C. Zietz, K. Arndt, R. Bogdanowicz, B. Nebe, R. Bader, A. Podbielski, Z. Hubicka, R. Hippler, Mater. Sci. Eng.: C 31 (2011) 1512–1519.
[12] D. Wojcieszak, M. Mazur, D. Kaczmarek, B. Szponar, M. Grobelny, M. Kalisz, A. Pelczarska, I. Szczygiel, A. Poniedzialek, M. Osekowska, Appl. Surf. Sci. (2016) 159–164.
[13] S. Achache, S. Lamri, A. Alhussein, A. Billard, M. François, F. Sanchette, Mater. Sci. Eng.: A 673 (2016) 492–502.
[14] S. Achache, S. Lamri, M. Arab Pour Yazdi, A. Billard, M. François, F. Sanchette, Surf. Coat. Technol. 275 (2015) 283–288.
[15] S. Achache, A. Alhussein, S. Lamri, M. François, F. Sanchette, C. Pulgarin, J. Kiwi, S. Rtimi, Colloids Surf. B: Biointerfaces (2016) 687–691.
[16] Kanagesan, M. Hashim, S. Tamilselvan, A. Ismail, K. Ahsanul, Adv. Mater. Sci. Eng. (2013) (Art. 710432).
[17] H.A. Jeng, J. Swanson, J. Environ. Sci. Health Part A 41 (2006) 2699–2711.
[18] Von Nägeli, Denkschrift. Allgemein. Naturforschung Ges. (1983) 174–182.
[19] E. Rentz, J. Nutr. Environ. Med. 13 (2003) 109–118.
[20] A. Nozik, Ann. Rev. Phys. Chem. 189 (1978) 521–549.
[21] A. Fujishima, X. Zhang, D. Tryk, Surf. Sci. Rep. 63 (2008) 515–546.
[22] E. Lipczynska-Kochany, J.R. Bolton, Env. Sci. Technol. 26 (1992) 259–261.
[23] X. Qiu, M. Miyaguchi, K. Sunada, M. Minoshima, M. Liu, Y. Lu, D. Li, Y. Shimodaira, Y. Hosogi, Y. Kiroda, K. Hashimoto, ACS Nano 6 (2012) 1609–1618.
[24] S. Rtimi, C. Pulgarin, R. Sanjines, V. Nadtochenko, J.-C. Lavanchy, J. Kiwi, Appl. Mater. Interfaces 7 (2015) 12832–12839.
[25] M. Ballo, S. Rtimi, S. Mancini, J. Kiwi, C. Pulgarin, J. Entenza, A. Bizzini, Appl. Microbiol. Biotechnol. 100 (2016) 5945–5953.
[26] O. Baghriche, S. Rtimi, A. Zertal, C. Pulgarin, R. Sanjinés, J. Kiwi, Appl. Catal. B 174–175 (2015) 376–382.
[27] A. Kraeutler, A. Bard, J. Am. Chem. Soc. 1100 (1978) 2244–2349.
[28] S. Rtimi, R. Sanjines, C. Pulgarin, J. Kiwi, J. Adv. Oxid. Technol. 20 (2017) 1.